NANO LETTERS
Letter
Cite This: Nano Lett. 2019, 19, 1039−1043
pubs.acs.org/NanoLett

Supercurrent Flow in Multiterminal Graphene Josephson Junctions

Anne W. Draelos,[†,‡] Ming-Tso Wei,[†] Andrew Seredinski,[†] Hengming Li,[†] Yash Mehta,[†] Kenji Watanabe,[§] Takashi Taniguchi,[§] Ivan V. Borzenets,[∥] Francois Amet,[‡] and Gleb Finkelstein[†,*]

[†]Department of Physics, Duke University, Durham, North Carolina 27708, United States
[‡]Department of Physics and Astronomy, Appalachian State University, Boone, North Carolina 28607, United States
[§]Advanced Materials Laboratory, NIMS, Tsukuba 305-0044, Japan
[∥]Department of Physics, City University of Hong Kong, Kowloon, Hong Kong SAR

* Supporting Information

ABSTRACT: We investigate the electronic properties of ballistic planar Josephson junctions with multiple superconducting terminals. Our devices consist of monolayer graphene encapsulated in boron nitride with molybdenum−rhenium contacts. Resistance measurements yield multiple resonant features, which are attributed to supercurrent flow among adjacent and nonadjacent Josephson junctions. In particular, we find that superconducting and dissipative currents coexist within the same region of graphene. We show that the presence of dissipative currents primarily results in electron heating and estimate the associated temperature rise. We find that the electrons in encapsulated graphene are efficiently cooled through the electron−phonon coupling.

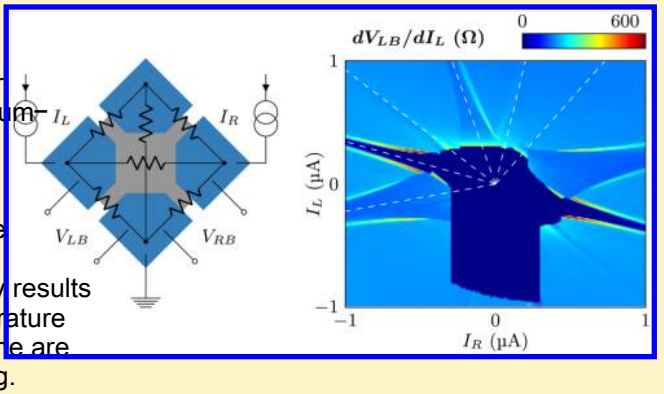

KEYWORDS: Graphene, superconductivity, ballistic Josephson junctions, multiterminal current flow, electron−phonon coupling

Superconducting proximity effects in graphene-based superconductor−normal−superconductor (SNS) devices attracted researchers' attention early on.[1−3] Ultraclean suspended graphene and heterostructures of graphene encapsulated in boron nitride further enable the study of proximity-induced superconductivity in the ballistic regime.[4−8] While these and following works investigated supercurrent flow in two-terminal junctions, here we are interested in more complex SNS structures where a normal metal is proximitized by several superconducting electrodes.

In such devices, the interplay of supercurrent flow involving different pairs of superconducting contacts could be highly nontrivial. For example, in a simple four-terminal configuration, biasing one terminal with respect to an adjacent terminal has been predicted to induce a "phase drag" between the other two terminals.[9,10] Furthermore, the energy spectrum of a multiterminal SNS device can emulate a band structure, where the superconducting phases play the role of quasi-momenta of a "crystal" of arbitrary dimension.[11−14] This effective band structure can accommodate Weyl points, and multiterminal Josephson junctions are therefore expected to provide insights into the physics of topological materials. On the experimental side, topological properties of multiterminal structures have been investigated in refs 15 and 16. Elsewhere, it has been reported that complex spectra of Andreev reflections could originate from nonlocal entanglement of two or more Cooper pairs in three or more leads.[17−20]

Encapsulated graphene is especially promising for the investigation of multiterminal SNS devices. Indeed, clean encapsulated samples are ballistic and could enable efficient Josephson coupling between superconducting contacts separated by several microns.[8] Here we report on the first observation of complex supercurrent flow in a four-terminal graphene SNS device. Our findings include a highly unusual coexistence of superconducting and dissipative currents in the same physical location.

The fabrication of these devices was detailed in prior works, which showed ballistic supercurrents in Josephson junctions up to 2 μm long.[8,21] Exfoliated monolayer graphene is encapsulated with hexagonal boron nitride using a standard stamping method.[22] The resulting stack is placed onto a p-doped silicon substrate with a 300 nm oxide layer. Carrier density in the graphene is controlled by a back gate voltage V_G. (Here we present data taken at V_G = 5 V. See Supporting Information for measurements at different gate values.) After an anneal in an argon/oxygen mixture, the stack is patterned with electron-beam lithography and then cut by reactive-ion etching to form the desired square mesa (3 μm × 3 μm). Contact electrodes are patterned on each corner, followed by a self-aligned etch and deposition of molybdenum−rhenium.

Received: October 27, 2018
Revised: December 23, 2018
Published: January 8, 2019

DOI: 10.1021/acs.nanolett.8b04330
Nano Lett. 2019, 19, 1039−1043

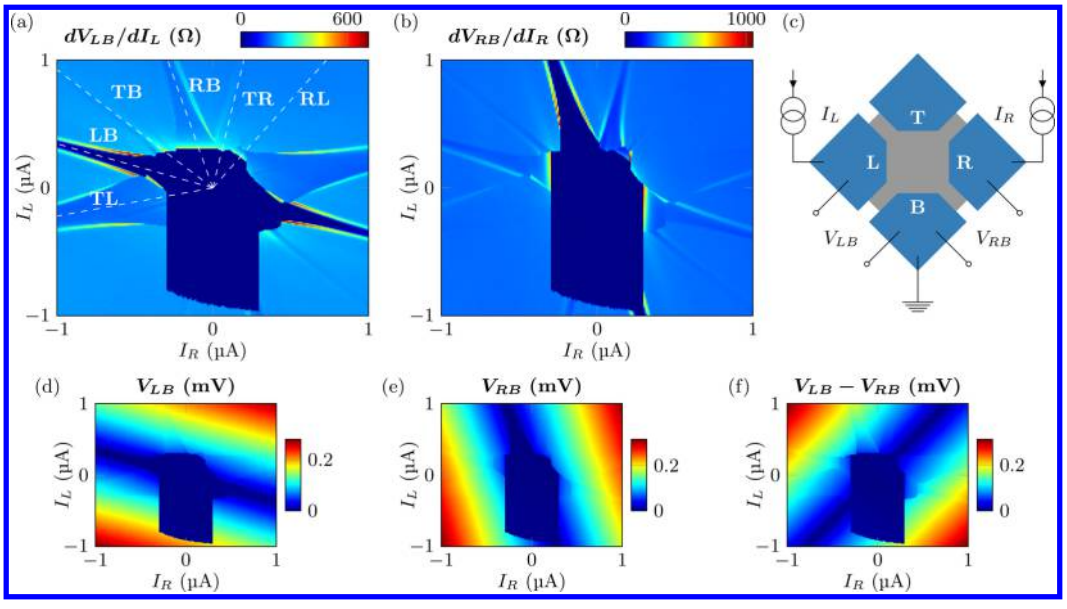

Figure 1. (a,b) Differential resistances dV_{LB}/dI_L and dV_{RB}/dI_R, measured at V_G = 5 V in the setup shown in (c). The darkest region in the center of both figures corresponds to the supercurrent across the whole sample. Maps were obtained by setting a single value of I_R and sweeping I_L from positive to negative values. The resulting superconducting region in the center of the maps is asymmetric in shape and extends further to negative due to the hysteresis between the retrapping and switching transitions (into and out of the superconducting state). Arm-shaped dark regions of resistance extend from the central rectangle (dashed lines) and show that they correspond to supercurrent flowing only between some pairs of terminals, as labeled. (c) Diagram of the sample with four superconducting terminals (blue) contacting a shared graphene region (gray). In the primary measurement configuration, currents I_L and I_R are sourced from the left and right contacts to the grounded bottom contact. Voltage difference between any two terminals could then be measured, such as V_{LB} and V_{RB}, the left-bottom and right-bottom voltage difference. (d, e) dc voltage maps of V_{LB} and $|V_{RB}|$ measured concurrently with the differential resistances maps in (a) and (b), respectively. It is clear that the orientation of the lines V_{LB} = 0 and V_{RB} = 0 (darkest blue) coincides with the major features in the differential resistance maps (a) and (b). (f) Map of the voltage difference between the left and the right contacts, $|V_{LR}|$. The line of equal voltage, V_{LR} = 0 runs diagonally from bottom left to top right, and a faint feature at the same location is also visible in the maps in (a,b).

The electrodes are ~100 nm thick and have a critical field of at least 9 T, a critical temperature of T_c ~ 10 K, and a measured superconducting gap Δ ~ 1.2 meV.[4,21] Each contact is 500 nm wide and is ~2 μm away from its adjacent neighbor at the closest point, and ~2 μm away from the contact diagonally across (see Supporting Information).

The samples were cooled in a Leiden Cryogenics dilution refrigerator to a base temperature of ~45 mK. Figure 1c shows a schematic of the transport measurement setup: two current sources were used, each combining a small ac excitation current of 10 nA and a dc bias up to ~1 μA (sufficient to switch a junction from the superconducting to the normal state). The bottom contact was grounded, and the top terminal remained floating, with no net current flowing through it. Two lock-in amplifiers set to noncommensurate frequencies (343.7 and 493.9 Hz) were used to measure the differential resistance of the left and right junctions, respectively. The dc voltage across a junction was concurrently measured, using a multichannel digital acquisition system (NI-6363 DAQ).

Figure 1a,b shows differential resistance maps of the left-bottom (LB) and right-bottom (RB) junctions as current is applied from both the left (I_L) and right (I_R) leads to the grounded bottom lead. In this way, the maps of the differential resistance $\frac{dV_{LB}}{dI_L}$ and $\frac{dV_{RB}}{dI_R}$ can be simultaneously measured as a function of both currents. A central dark region of zero resistance in both maps indicates supercurrent through the whole sample. Due to the difference between the switching and the retrapping currents, this region extends to the bottom part of the maps, which are measured with I_R held fixed while I_L is swept from positive to negative bias.

Beyond the central roughly rectangular feature, this superconducting region is additionally extended into several narrow diagonal "arms" of suppressed resistance. To help identify the origin of these arms, we plot the dc voltage across the left and right junctions, V_{LB} and V_{RB}. Figure 1d shows a line of zero voltage drop across the left-bottom junction, V_{LB} = 0, which naturally corresponds to the dominant arm of suppressed resistance in the resistance of the left-bottom junction (Figure 1a). Similarly, for the right bottom junction the dominant arm in Figure 1b is due to a zero voltage drop V_{RB} = 0 (Figure 1e). Both features result in resistance being suppressed to zero by the supercurrent flowing between the two contacts being measured. We furthermore find a fainter version of each feature in the complementary map: the LB pair turning superconducting affects the measured RB resistance and vice versa. Beyond these obvious supercurrent branches, we now show that the other arms found in Figure 1a,b correspond to superconducting coupling between other pairs of terminals.

Specifically, we find that these additional features are due to the incorporation of the top, ungrounded, and otherwise unused terminal. Keeping the sources and ground terminals the same and moving the voltage probes to the top and left/right junctions allows us to identify the remaining wide features in Figure 1b,c as the lines of equal dc voltage V_{TL} = 0 V and V_{TR} = 0. This condition indicates that the pairs of terminals top-left or top-right are coupled by a superconducting current. The relative strength of these features is

DOI: 10.1021/acs.nanolett.8b04330
Nano Lett. 2019, 19, 1039−1043

also understandable: the LB resistance $\frac{dV_{LB}}{dI_L}$ is strongly affected by the supercurrent in the adjacent TL junction with which it shares the left terminal (Figure 1b). However, the supercurrent in the TR junction has relatively less effect on LB because no terminals are directly shared, and the corresponding feature is faint. Instead, the supercurrent in the TR junction creates a prominent feature in the $\frac{dV_{RB}}{dI_R}$ map in Figure 1c, as the two junctions share the right terminal.

The maps also show two faint and narrow features labeled RL and TB, which we attribute to a superconducting coupling between diagonally opposite contacts. Indeed, the location of the RL line coincides with the condition $V_{RL} = 0$ visible in Figure 1f, which shows the V_{RL} map. It should be noted that the induced coherence length ($\xi \approx 500$ nm) is comparable to the distance between the neighboring superconducting contacts and smaller than the diagonal distances R-L and T-B.[8] Therefore, the supercurrents across the diagonals should be several times weaker than the supercurrents coupling the neighboring contacts. Nonetheless, the features corresponding to the supercurrent flowing along the sample diagonals are clearly observed. Furthermore, we surprisingly find areas of the maps in which only one pair of diagonally opposite contacts is coupled by a supercurrent, while the supercurrent between any other pair of contacts is suppressed. This means that a supercurrent could flow along one of the sample diagonals, while dissipative currents flow along the opposite diagonal and between any neighboring contacts.

To quantitatively understand the pattern of supercurrent flow, we examine a circuit diagram consisting of six Josephson junctions connecting the four terminals (Figure 2a). Away from the central superconducting region of the map in Figure 1a,b, the diagonal arms of suppressed resistance correspond to one of the junctions turning superconducting (i.e., its resistance in the network model is switched to zero), while the rest remain resistive. By measuring $\frac{dV_{LB}}{dI_L}$ and $\frac{dV_{RB}}{dI_R}$ when the system is fully resistive and when some of the junctions are in the superconducting state, we can construct a system of equations allowing us to solve for the normal resistances of all junctions. We find that the neighboring leads are effectively coupled by ~300 Ω, while the diagonal resistances are ~1.5−2 kΩ.

Once the normal state resistances are determined and the critical currents I_C of each junction are estimated from the maps, we can model the current flow in the system.[23] The network includes six resistively shunted junctions (RSJ), consisting of a normal resistor (Figure 2a) in parallel with a junction of critical current I_C. Parts b and c of Figure 2 show the resultant maps of differential resistance for the left and right junctions, corresponding to the experimental maps in Figure 1a,b. The model captures the overall features of the experiment, such as the existence of the central superconducting region and the extending diagonal "arms". The values of the resistance in the arms, as well as the slopes of the arms, are constrained by our extracted values of the network resistors. Note that in our model the diagonal junctions TB and RL do not directly interact, even though they share the same physical space. This assumes that the coexisting dissipative and superconducting currents do not strongly interfere with each other.

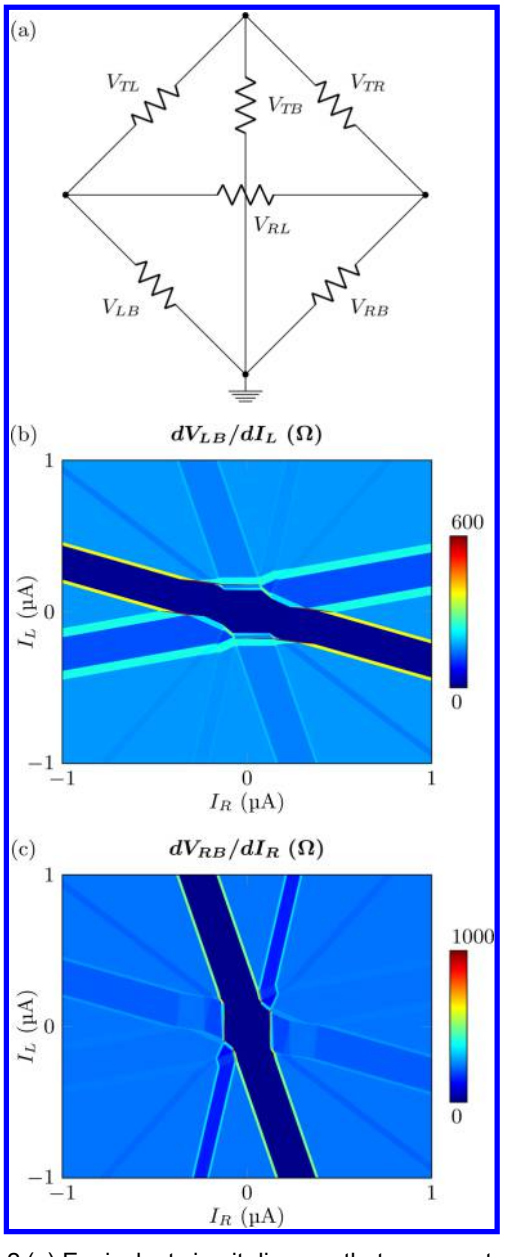

Figure 2. (a) Equivalent circuit diagram that represents the coupling between each pair of terminals as a resistor. Each resistor could be replaced with an effective short to indicate a superconducting coupling between the corresponding pair of terminals, and consequently, the locally measured voltage would be zero. (b, c) Maps of differential resistance for the left bottom and right bottom junctions, respectively, generated from a numerical simulation. The six major features in Figure 1a,b are realistically reproduced in both maps, with lines of equal voltage appearing at certain orientations within the I_L−I_R plane.

While all six of the supercurrent arms are reproduced in this model, the decay of I_C at higher bias currents is not, because the model does not account for the effects of dissipation within the device. Indeed, it has been previously shown that the critical current of an SNS structure is strongly affected by self-heating.[24] Some of us have explored this effect in graphene-based structures.[26] To quantify the effects of Joule heating in the present device, we measure similar maps of differential resistance at different substrate temperatures. From such maps, we extract the value of the critical current in the measured

DOI: 10.1021/acs.nanolett.8b04330
Nano Lett. 2019, 19, 1039−1043

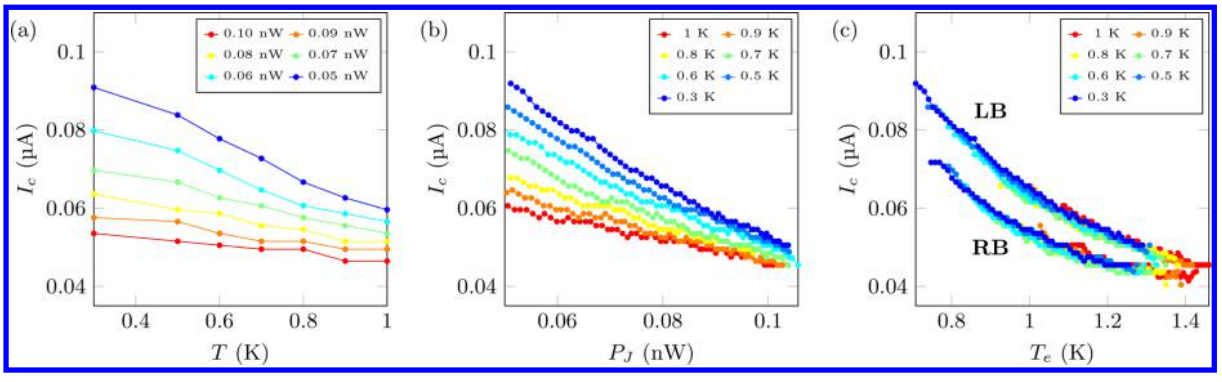

Figure 3. (a,b) Critical current in the LB junction plotted as a function of the substrate temperature and heating power, respectively. For a given substrate temperature, we extract the dependence of the critical current I_C (measured along the I_L axis) on the heating current I_R. The heating power P_J is calculated as the product of I_R and V_R (measured separately). (c) Critical current in the LB (top curves) and RB (bottom curves) junctions, plotted as a function of electron temperature, T_e. T_e is calculated from the equilibrium between Joule heating and electron−phonon cooling as $(T^\delta + P_J/\Sigma)^{1/\delta}$. Importantly, the same Σ is used for both junctions. The observed universal behavior shows how the decay of each superconducting branch can be attributed solely to electron heating.

junction as a function of the substrate temperature T (Figure 3a). The different curves correspond to different applied heating power P_J, calculated as $I_R V_R$ to represent the Joule heating due to the right current when the left junction is superconducting. Figure 3b represents the same data plotted vs P_J at different T. Clearly, I_C is suppressed by both P_J and T.

While the dissipative currents heat the electron system, superconducting gap relative to the low bias in the contacts prevents the efficient cooling by outflow of hot electrons.[25−27] As a result, heat can only dissipate via the relatively inefficient electron−phonon coupling. The power dissipated through electron−phonon cooling scales like $P_{e-ph} = \Sigma(T_e^\delta - T^\delta)$, where Σ is the electron phonon coupling constant integrated over the area of the device, T_e is the temperature of the electron system, and T is the phonon bath temperature, assumed to be unaffected by the dissipated heat and to equal the substrate temperature. The exponent δ could be 3 or 4 depending on the temperature range and the mean free path; for a recent summary of the literature, see ref 28. If all the Joule heat is dissipated via phonons, the electron temperature at equilibrium is expected to reach $T_e = (T^\delta + P_J/\Sigma)^{1/\delta}$. Using a single fitting parameter Σ, we can show that the critical current I_C in both the LB and RB junctions scales universally as a function of the equilibrium electron temperature, T_e, = $(T^3 + P_J/\Sigma)^{1/3}$ (Figure 3e). Here, we used $\delta = 3$; we have found that taking $\delta = 4$ does not allow us to successfully scale the data. Σ is found to be 30 pW/K^3 (or scaled per graphene area ~10 W/m^2 K^3), which is significantly larger than the results found in nonencapsulated graphene.[28] We speculate that the more efficient cooling in our case could be explained either by scattering at the edges of the graphene crystal, which could momentum relaxation, or by direct emission of phonons into the BN substrate, both of which enhance electron−phonon scattering.[29]

The presence of a dissipative current in a SNS structure could create an effectively thermal distribution at an elevated electron temperature or lead to a genuinely nonequilibrium electron distribution, which could manifest itself in, e.g., a reversal of the supercurrent.[30−33] In our experiment, no such nonequilibrium effects were observed.

Additional measurements would be required to search for any change of the current-phase relation in our samples.

In summary, we have experimentally studied the complex supercurrent flow in a four-terminal graphene SNS junction. We explained the six distinct branches that appear in the resistance maps. Interestingly, we have observed the regime where supercurrent and dissipative current coexist in the same area of graphene. The results could be successfully modeled with a network of six shunted Josephson junctions. Finally, the effects of the dissipative current on the magnitude of the supercurrent can be accounted for by self-heating in the device. Our experiment opens the prospects for future search of topological effects in multiterminal graphene devices.[11−16]

ASSOCIATED CONTENT

Supporting Information

The Supporting Information is available free of charge on the ACS Publications website at DOI: 10.1021/acs.nanolett.8b04330.

Details of sample characterization including optical images of samples, gate dependence of R_N, and votage vs I_{bias} map. Demonstration of the ballistic nature of the graphene via supercurrent scaling analysis. Alternative measurement configurations including data taken at different gate voltages, direct voltage measurement between top and bottom electrodes, rotated sample orientation, and interchanged bias sweep order. Additional SPICE simulations with a table of resistor values and simulated maps for R and imbalances (PDF)

AUTHOR INFORMATION

Corresponding Authors
*E-mail: iborzene@cityu.edu.hk.
*E-mail: gleb@phy.duke.edu.
ORCID
Kenji Watanabe: 0000-0003-3701-8119
Ivan V. Borzenets: 0000-0002-1577-8312

Notes

The authors declare no competing financial interest.

ACKNOWLEDGMENTS

Low temperature electronic measurements performed by A.W.D. and G.F. were supported by the Division of Materials Sciences and Engineering, Office of Basic Energy Sciences, U.S.

DOI: 10.1021/acs.nanolett.8b04330
Nano Lett. 2019, 19, 1039−1043

[redacted]5 thographic fabrication and characterization of the samples performed by M.T.W. and A.S. were supported by [redacted] 22 a[redacted]13 [redacted]F.A. acknowledges the ARO under Award W911NF-16-1-0132. I.V.B. acknowledges City U New Research Initiatives/Infrastructure Support from Central (APRC): 9610395. This work was performed in part at the Duke University Shared Materials Instrumentation Facility (SMIF), a member of the North Carolina Research Triangle Nanotechnology Network (RTNN), which is supported by the National Science Foundation (Grant ECCS-1542015) as part of the National Nanotechnology Coordinated Infrastructure (NNCI). K.W. and T.T. acknowledge support from JSPS KAKENHI Grant No. JP15K21722 and the Elemental Strategy Initiative conducted by the MEXT, Japan. T. T. acknowledges support from JSPS Grant-in-Aid for Scientific Research A (No. 26248061) and JSPS Innovative Areas 'Nano Informatics' (No. 25106006).

REFERENCES

(1) Heersche, H. B.; Jarillo-Herrero, P.; Oostinga, J. B.; Vandersypen, L. M. K.; Morpurgo, A. F. Bipolar supercurrent in graphene. Nature 2007, 446, 56.
(2) Miao, F.; Wijeratne, S.; Zhang, Y.; Coskun, U. C.; Bao, W.; Lau, C. N. Phase-Coherent Transport in Graphene Quantum Billiards. Science 2007, 317 (5844), 1530.
(3) Du, X.; Skachko, I.; Andrei, E. Y. Josephson current and multiple Andreev reflections in graphene SNS junctions. Phys. Rev. B: Condens. Matter Mater. Phys. 2008, 77, 184507.
(4) Calado, V. E.; Goswami, S.; Nanda, G.; Diez, M.; Akhmerov, A. R.; Watanabe, K.; Taniguchi, T.; Klapwijk, T. M.; Vandersypen, L. M. K. Ballistic Josephson junctions in edge-contacted graphene. Nat. Nanotechnol. 2015, 10, 761.
(5) Ben Shalom, M.; Zhu, M. J.; Fal'ko, V. I.; Mishchenko, A.; Kretinin, A. V.; Novoselov, K. S.; Woods, C. R.; Watanabe, K.; Taniguchi, T.; Geim, A. K.; Prance, J. R. Quantum oscillations of the critical current and high-field superconducting proximity in ballistic graphene. Nat. Phys. 2016, 12, 318.
(6) Allen, M. T.; Shtanko, O.; Fulga, I. C.; Akhmerov, A. R.; Watanabe, K.; Taniguchi, T.; Jarillo-Herrero, P.; Levitov, L. S.; Yacoby, A. Spatially resolved edge currents and guided-wave electronic states in graphene. Nat. Phys. 2016, 12, 128.
(7) Kumaravadivel, P.; Du, X. Signatures of evanescent transport in ballistic suspended graphene-superconductor junctions. Sci. Rep. 2016, 6, 24274.
(8) Borzenets, I. V.; Amet, F.; Ke, C. T.; Draelos, A. W.; Wei, M. T.; Seredinski, A.; Watanabe, K.; Taniguchi, T.; Bomze, Y.; Yamamoto, M.; Tarucha, S.; Finkelstein, G. Ballistic Graphene Josephson Junctions from the Short to the Long Junction Regime. Phys. Rev. Lett. 2016, 117, 237002.
(9) Omelyanchouk, A. N.; Zareyan, M. Ballistic four-terminal Josephson junction: bistable states and magnetic flux frustration. Physica B Condens. Matter 2000, 291, 81.
(10) Amin, M. H. S.; Omelyanchouk, A. N.; Zagoskin, A. M. Mesoscopic multiterminal Josephson structures I. Effects of nonlocal weak coupling. Low Temp. Phys. 2001, 27, 616.
(11) Mai, S.; Kandelaki, E.; Volkov, A.; Efetov, K. Stationary Josephson effect in a short multiterminal junction. Phys. Rev. B: Condens. Matter Mater. Phys. 2013, 87, 024507.
(12) Riwar, R.-P.; Houzet, M.; Meyer, J. S.; Nazarov, Y. V. Multi-terminal Josephson junctions as topological matter. Nat. Commun. 2016, 7, 11167.
(13) Eriksson, E.; Riwar, R.-P.; Houzet, M.; Meyer, J. S.; Nazarov, Y. V. Topological transconductance quantization in a four-terminal Josephson junction. Phys. Rev. B: Condens. Matter Mater. Phys. 2017, 95, 075417.
(14) Xie, H.-Y.; Vavilov, M. G.; Levchenko, A. Topological Andreev bands in three-terminal Josephson junctions. Phys. Rev. B: Condens. Matter Mater. Phys. 2017, 96, 161406.
(15) Strambini, E.; D'Ambrosio, S.; Vischi, F.; Bergeret, F. S.; Nazarov, Y. V.; Giazotto, F. The ω-SQUIPT as a tool to phase-engineer Josephson topological materials. Nat. Nanotechnol. 2016, 11, 1055.
(16) Vischi, F.; Carrega, M.; Strambini, E.; D'Ambrosio, S.; Bergeret, F. S.; Nazarov, Y. V.; Giazotto, F. Coherent transport properties of a three-terminal hybrid superconducting interferometer. Phys. Rev. B: Condens. Matter Mater. Phys. 2017, 95, 054504.
(17) Freyn, A.; Doucot, B.; Feinberg, D.; Melin, R. Production of Nonlocal Quartets and Phase-Sensitive Entanglement in a Superconducting Beam Splitter. Phys. Rev. Lett. 2011, 106, 257005.
(18) Jonckheere, T.; Rech, J.; Martin, T.; Doucot, B.; Feinberg, D.; Melin, R. Multipair dc Josephson resonances in a biased all-superconducting bijunction. Phys. Rev. B: Condens. Matter Mater. Phys. 2013, 87, 214501.
(19) Pfeffer, A. H.; Duvauchelle, J. E.; Courtois, H.; Melin, R.; Feinberg, D.; Lefloch, F. Subgap structure in the conductance of a three-terminal Josephson junction. Phys. Rev. B: Condens. Matter Mater. Phys. 2014, 90, 075401.
(20) Cohen, Y.; Ronen, Y.; Kang, J.-H.; Heiblum, M.; Feinberg, D.; Melin, R.; Shtrikman, H. Nonlocal supercurrent of quartets in a three-terminal Josephson junction. Proc. Natl. Acad. Sci. U. S. A. 2018, 115, 6991.
(21) Amet, F.; Ke, C.-T.; Borzenets, I. V.; Wang, J.; Watanabe, K.; Taniguchi, T.; Deacon, R. S.; Yamamoto, M.; Bomze, Y. V.; Tarucha, S.; Finkelstein, G. Supercurrent in the quantum Hall regime. Science 2016, 352 (6288), 966.
(22) Wang, L.; Meric, I.; Huang, P. Y.; Gao, Q.; Gao, Y.; Tran, H.; Taniguchi, T.; Watanabe, K.; Campos, L. M.; Muller, D.; Guo, J.; Kim, P.; Hone, J.; Shepard, K. L.; Dean, C. R. One-Dimensional Electrical Contact to a Two-Dimensional Material. Science 2013, 342 (6158), 614.
(23) The network was modeled using Simulation Program with Integrated Circuit Emphasis (SPICE).
(24) Courtois, H.; Meschke, M.; Peltonen, J. T.; Pekola, J. P. Origin of Hysteresis in a Proximity Josephson Junction. Phys. Rev. Lett. 2008, 101, 067002.
(25) Voutilainen, J.; Fay, A.; HÃd'kkinen, P.; Viljas, J. K.; HeikkilÃd', T. T.; Hakonen, P. J. Energy relaxation in graphene and its measurement with supercurrent. Phys. Rev. B: Condens. Matter Mater. Phys. 2011, 84, 045419.
(26) Borzenets, I. V.; Coskun, U. C.; Mebrahtu, H. T.; Bomze, Y. V.; Smirnov, A. I.; Finkelstein, G. Phonon Bottleneck in Graphene-Based Josephson Junctions at Millikelvin Temperatures. Phys. Rev. Lett. 2013, 111, 027001.
(27) Betz, A. C.; Jhang, S. H.; Pallecchi, E.; Ferreira, R.; FÃ¨ve, G.; Berroir, J. M.; Placais, B. Supercollision cooling in undoped graphene. Nat. Phys. 2013, 9, 109.
(28) McKitterick, C. B.; Prober, D. E. Electron-phonon cooling in large monolayer graphene devices. Phys. Rev. B: Condens. Matter Mater. Phys. 2016, 93, 075410.
(29) Kong, J. F.; Levitov, L.; Halbertal, D.; Zeldov, E. Resonant electron-lattice cooling in graphene. Phys. Rev. B: Condens. Matter Mater. Phys. 2018, 97, 245416.
(30) Morpurgo, A. F.; Klapwijk, T. M.; van Wees, B. J. Hot electron tunable supercurrent. Appl. Phys. Lett. 1998, 72, 966.
(31) Giazotto, F.; Heikkila, T. T.; Taddei, F.; Fazio, R.; Pekola, J. P.; Beltram, F. Tailoring Josephson Coupling through Superconductivity-Induced Nonequilibrium. Phys. Rev. Lett. 2004, 92, 137001.
(32) Baselmans, J. J. A.; Morpurgo, A. F.; Van Wees, B. J.; Klapwijk, T. M. Reversing the direction of the supercurrent in a controllable Josephson junction. Nature 1999, 397, 43.
(33) Baselmans, J. J. A.; Morpurgo, A. F.; Van Wees, B. J.; Klapwijk, T. M. Tunable supercurrent in superconductor/normal metal/superconductor Josephson junctions. Superlattices Microstruct. 1999, 25 (5), 973.

DOI: 10.1021/acs.nanolett.8b04330
Nano Lett. 2019, 19, 1039−1043